1-1-2003

In situ reactive blending to prepare polystyrene-clay and polypropylene-clay nanocomposites

Dongyan Wang
Marquette University

Charles A. Wilkie
Marquette University, charles.wilkie@marquette.edu

Accepted version. *Polymer Degradation and Stability*, Vol. 80, No. 1 (2003): 171-182. DOI.

Polymer Degradation and Stability, Vol. 80, No. 1 (2003): 171-182. DOI.

In-situ Reactive Blending to Prepare polystyrene–clay and Polypropylene–clay Nanocomposites

Dongyan Wang

Department of Chemistry, Marquette University, Milwaukee, WI

Charles A. Wilkie

Department of Chemistry, Marquette University, Milwaukee, WI

Abstract

Nanocomposites of polystyrene and polypropylene with organically-modified clay may be prepared by melt blending in a Brabender mixer the clay and the polymer. The presence of maleic anhydride increases the likelihood of nanocomposite formation for polystyrene but is less important for polypropylene. The materials that result are immiscible materials, in that the clay is not uniformly distributed throughout the polymer matrix, but there is polymer inserted between the clay layers. The results from cone calorimetry suggest that nanocomposite formation has occurred, since there is a significant reduction in the peak heat release rate.

1. Introduction

The study of polymer clay nanocomposites has been an active research field in polymer chemistry and material science for the past decade [1], [2], [3]. These materials are of interest because of the enhanced mechanical and thermal properties and the decrease in permeability. The combination of a nano-dimensional material with a polymer may yield either an immiscible material, in which the clay is acting as a filler and is not dispersed at the nanometer level, or a nanocomposite may be obtained. If the registry between the clay layers is maintained, the material is described as intercalated, while, if this registry is lost, the material is called exfoliated, also known as delaminated. Nanocomposites may be prepared either by polymerization or by a blending process. Bulk or in situ polymerization has also been used and frequently this offers better dispersion of the clay than can be obtained by a blending process, but there is a synthetic expense. The advantage of the polymerization process may be that the monomer is inserted into the gallery space of the clay where it undergoes polymerization, giving intercalated or exfoliated polymer clay nanocomposites. For a blending process, one must depend upon shear forces to drive the polymer between the clay layers and it is likely to be more difficult to insert polymer than monomer.

Clay contains layered silicate sheets, on which there resides a negative charge, and this is balanced by the charge on cations, typically sodium cations, within the gallery space; thus the gallery space is quite hydrophilic. Polymers and solvents which exhibits hydrophilic properties, such as poly(tetrahydrofuran) (THF) [4], thiophene [5], epoxy [6], poly(vinyl chloride) (PVC) [7], [8], poly(ethylene oxide) (PEO) [9], etc, can directly insert into the gallery space of the natural-occurring clay and may form an intercalated or exfoliated nanocomposite. For the majority of polymers, owing to their hydrophobic character, the clay must be modified with a surfactant in order to make the gallery space sufficiently hydrophobic to permit it to interact with the polymer. Another possibility is to use a compatibilizer, which would enhance the compatibility between the polymer and the sodium or organically-modified clay.

Polystyrene (PS) clay nanocomposite have been prepared by both the in-situ polymerization method and melt intercalation. Zhu et al. [10] prepared both intercalated and exfoliated structure polystyrene clay nanocomposites using a bulk polymerization technique; the structure of the nanocomposite, intercalated or exfoliated, depends on the nature of the ‘onium’ counterion. Tseng et al. [11] reported the preparation of syndiotactic polystyrene/modified-clay nanocomposites by solution blending a mixture of pure s-PS and an organophilic clay in dichlorobenzene. PS–clay nanocomposites were also prepared by free radical polymerization of styrene containing vinylbenzyldimethyldodecylammonium as the surfactant [12] while PS-sodium clay nanocomposites were prepared by emulsion polymerization [13]. A comparison of solution, emulsion, suspension and bulk polymerization along with melt blending has also been performed [14].

Zeng et al. [15], [16] prepared (PS) clay nanocomposites via *in-situ* bulk polymerization; the effects of initiators and clay surface chemical modification on the nanocomposite structures were studied. They prepared a masterbatch, containing high clay content, by bulk polymerization and then used a compounder to lower the clay concentration.

A shear-induced ordered structure in an exfoliated PS/clay nanocomposite was reported by Chen et al. [17]. Self-assembly of a shear-induced ordered structure in the nanocomposite was reported for the first time. The self-assembly behavior was measured by XRD patterns, TEM, and FTIR dichroism technique. Compared with the broad amorphous peaks of the PS, a series of sharp XRD peaks were observed for the extruded PS/clay nanocomposite pellet sample, showing that an ordered structure occurred under shear flow.

Park et al. [18] reported the fabrication of nanocomposite of syndiotactic polystyrene (sPS)/organophilic clay conducted by melt intercalation. To avoid the decrease of interlayer spacing due to desorption of organic materials at high temperature, various amorphous styrenic polymers were introduced during the melt mixing

process. The mechanical properties of the nanocomposites such as tensile strength, flexural modulus and izod impact strength were measured and discussed in relation to their microstructures.

Liu et al. [19] prepared polypropylene (PP)/clay nanocomposites via graft copolymerization-melt compounding by using a new organophilic clay which had a larger interlayer spacing than the ordinarily organophilic clay only modified by alkyl ammonium. This larger interlayer spacing was accomplished by co-intercalation of monomers into the organoclay. One of the co-intercalation monomers was unsaturated, so it could tether on the PP backbone by a graft copolymerization reaction. The mechanical properties of the PP nanocomposite were improved. Nam et al. [20] prepared intercalated PP/clay nanocomposites using maleic anhydride (MA) modified PP (PP-g-MA) and an organophilic clay via melt extrusion process. The intercalated PP nanocomposites showed an enhancement of modulus compared with PP matrix without clay.

Okamoto et al. [21] conducted foam processing on PP/clay nanocomposite in a batch process in an autoclave using supercritical CO_2 as foaming agent under 10 MPa at 134.7 °C. Kodgire et al. [22] studied the morphology and properties of PP/clay nanocomposites. The melt intercalation of organophilic clay was carried out with a single-screw extruder and PP-g-MA was used as a compatibilizer. Hambir et al. [23] studied the disordered structure of PP/octadecylamine-modified montmorillonite clay nanocomposites. The onset of thermal degradation temperature increased from 270 °C to about 330 °C. The DMA data show significant improvement in the storage modulus; the intensity of the loss modulus peak decreased, showing weak cooperative relaxation of PP in the PP/clay composites. Kim et al. [24] prepared a polymer layered organosilicate nanocomposite by simple melt mixing of PP, PP-g-MA and organically modified clay. The nanocomposite exhibits higher thermal stability compared to the blend composed of PP and PP-g-MA only. The rheology of nanocomposite was also investigated. Lee et al. [25] employed a polyethylene glycol (PEG) oligomer in addition to PP-g-MA to improve both the intercalation of polymers and the compatibility with the PP matrix. The hybrid composites containing PP-g-MA (or PP), PEG and montmorillonite were prepared using a mixer and fabricated into thin film with a hot press. The intercalation of polymers between the clays was quite improved by the addition of the PEG oligomers. Kurokawa et al. [26] prepared a PP nanocomposite using PP-g-MA with an organically-modified clay which was then blended with PP to reduce the clay content.

This study examines the effect of the particular organic modification of the clay, the effect of maleic anhydride, and the effect of shear on the formation of PP and PS nanocomposites by melt blending. Nanocomposite formation is followed using X-ray diffraction, transmission electron microscopy, thermogravimetric analysis, cone calorimetry and the evaluation of mechanical properties.

2. Experimental

2.1. Materials

Dimethylhydrogenatedtallowbenzylammonium chloride was kindly provided by Akzo Nobel Surface Chemistry LLC and the organically-modified clay containing this cation, Cloisite 10A, was provided by Southern Clay Products. The sodium clay was provided by both Southern Clay and by Nanocor; the Southern Clay material was used for mixing in the Brabender mixer while the Nanocor material was used in the higher shear mixing devices. Dimethylhexadecylstyrylammonium chloride and the clay containing this cation were synthesized following procedures that have been previously published [4]. Polystyrene was acquired from the Aldrich Chemical Company; it has a Melt Flow Index (200 °C/5 kg, ASTM D 1238) 7.5 g/10 min, average molecular weight Mw ca. 230,000 and Mn ca 140,000. Polypropylene (i-PP) is also an Aldrich product; it has a Melt Flow Index (230 °C/2.16 kg, ASTM D 1238) 35 g/10min, average molecular weight Mw ca. 190,000 and Mn ca. 50,000. All purchased materials are used as received.

2.2. In-situ reactive blending

For the organic clay systems, 50 g of commercial PS or PP was mixed with 1.5 g of organic clay, either VB16 clay or 10A clay, then the mixture was melt blended in Brabender Plasti-Cord (cell volume is 50 cm^3) at 200 °C with high rotor speed (60 rpm) for 30 min either in the presence or absence of maleic anhydride (MA, 1.5 g).

For the sodium clay systems, 50 g of commercial PS or PP, 1.5 g of sodium clay, 0.5 g of ammonium salt—either 10A or VB16 salt was dry mixed and then the mixture was melt blended in Brabender Plasti-Cord at 200 °C with high rotor speed (60 rpm) for 30 min either in the presence or absence of 1.5 g of MA.

Both preparations were also performed using an internal mixer (herein denoted as intermixer), which has a cell volume of 200 cm^3 at a rotor speed of 100 rpm at 200 °C for PS and 100 rmp at 190 °C for PP. A twin-screw extruder (L/D ratio 20/1) was also utilized; the barrel temperature distribution was 180 °C, 200 °C, 200 °C and 190 °C from feeder to extrusion-head and the screw speed were 50 rpm for PS, for PP the values were 170 °C, 190 °C, 190 °C, 180 °C and 50 rpm.

2.3. Instrumentation

X-ray diffraction (XRD) patterns were obtained using a Rigaku Geiger Flex, 2-circle powder difractometer equipped with Cu-K_α generator (λ=1.5404 Å). Generator tension is 50 KV and generator current is 20 mA. All the samples were compress molded at 170–180 °C to 20 mm × 15 mm × 1 mm plaques for XRD measurements. Thermogravimetric analysis (TGA) was performed on a Cahn TG131 unit under a 30ml/min flowing nitrogen atmosphere at a scan rate of 10 °C/min from 20 °C to 600 °C; temperatures are reproducible to ±3 °C and the fraction of non-volatile residue to ±2%. TGA-FTIR was performed on a Cahn TG131 unit coupled to a Mattson Research Series FTIR spectrometer under a 60 ml/min flow nitrogen atmosphere at a scan rate of 30 °C/min from 200 °C to 600 °C. Mechanical properties, tensile strength and elongation at break, were measured using dumbbell samples cut from about 0.3 mm thickness thin films according to ASTM D882-75b on an Instron Universal Test Machine. The crosshead speed was 5 mm/min or 1.25 mm/min, and five specimens were tested for each sample. Bright field transmission electron microscopy (TEM) image was obtained at 120 kV, at low-dose conditions, with a Phillips 400T electron microscopy. The sample was ultramicrotomed with a diamond knife on a Leica Ultracur UCT microtome at room temperature to give 70-nm-thick section. The section was transferred from water to carbon-coated Cu grids of 200 mesh. The contrast between the layered silicate and the polymer phase was sufficient for imaging, so no heavy metal staining of sections prior to imaging was required. Cone calorimetry was performed on an Atlas CONE-2 according to ASTM E 1354-92 at an incident flux of 35 kW/m^2 using a cone shaped heater. Exhaust flow was set at 24 l/s and the spark was continuous until the sample ignited. Cone samples were prepared by compression molding the sample (about 30 g) into square plaques. Typical results from Cone calorimetry are reproducible to within about ±10%. These uncertainties are based on many runs in which thousands of samples have been combusted [27].

3. Results and discussion

3.1. X-ray diffraction (XRD)

XRD is an effective way to characterize the formation of a nanocomposite. In an immiscible mixture, the gallery height of clay, in terms of its d-spacing, should be virtually identical to that of the pristine clay; if a nanocomposite is formed, the d-spacing must increase. Two cases are possible, a peak is seen at larger d-spacing than in the pristine clay, indicating an intercalated structure, or no peak is seen, which may indicate either an exfoliated structure or disordering of the clay layers.

The first question to be addressed is the effect of MA on 2θ for PS systems using the devise which has the smallest shear, the Brabender mixer. Fig. 1 shows that for organically-modified 10A–clay, the simple melt

blending with PS results in a shift in 2θ that corresponds to a change in d-spacing from 1.9 to 3.5 nm. When MA is added, the change in d-spacing becomes somewhat smaller as the peak shifts to 3.2 nm, but the peak becomes much sharper. One interpretation of this is that there is more disordering in the absence of MA and the diffuse nature of the peak makes locating its center difficult. In the presence of MA, it seems clear that intercalation has occurred. Different results are obtained for VB16, as shown in Fig. 2. The d-spacing of the VB16–clay is 2.9 nm, after melt blending with PS, the d-spacing decreases to 2.1 nm. Once again the peak is quite diffuse so it is difficult to state the exact position of the peak. In the presence of MA, the peak position is changed, moving to 3.0 nm, a slight increase from that in the pristine clay, but the peak is now much sharper. It is obvious that MA has some effect but, based upon XRD information alone, one cannot identify this effect.

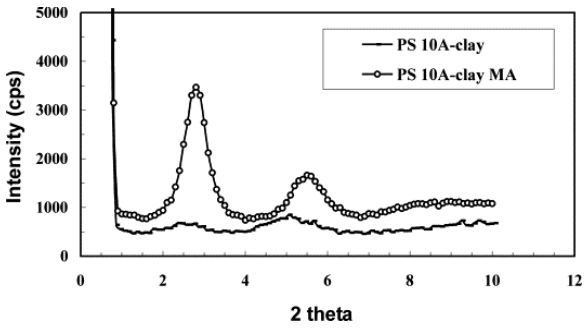

Fig. 1. XRD pattern of PS 10A–clay nanocomposite.

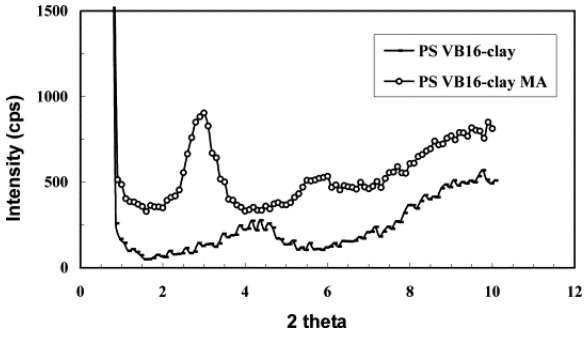

Fig. 2. XRD pattern of PS VB16–clay nanocomposite.

We will next examine the difference between the prior formation of the organically-modified clay versus melt blending the sodium clay together with the surfactant, again in the presence and absence of MA. The work of Alexandre et al. [28] has shown that one may form nanocomposites by blending of a sodium clay with a quaternary ammonium salt or by the direct use of the organically-modified clay. Fig. 3 shows the results using the 10A surfactant. The d-spacing for PS with the sodium clay and MA is 1.2 nm which shifts slightly in the presence of the 10A salt to 1.5 nm. It is significant to note that when all four components are present, PS, sodium clay, 10A salt and MA, the d-spacing increases to 2.8 nm. This is less than the values of 3.2–3.5 nm seen when the 10A clay is used directly but still is likely indicative of some nanocomposite formation. It must be noted that the peaks are much stronger when the organically-modified clay is directly used and this may imply more disorder in the sodium clay system.

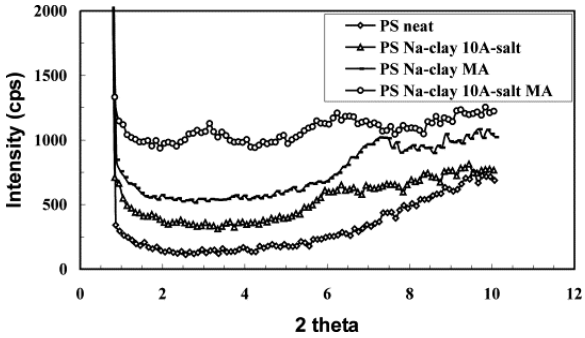

Fig. 3. XRD patterns of PS with 10A salt and sodium clay and the effect of MA.

Very similar results are seen for the VB16 system, shown in Fig. 4. It is interesting that, if one looks at the XRD patterns of Fig. 3, Fig. 4, both ammonium salts 10A and VB16 (PS Na–clay 10A-salt vs. PS Na–clay VB16-salt) show the same gallery spacing, 1.8 – 1.9 nm. When MA is present, the gallery spacing is again the same at 2.8 – 2.9 nm. When the organically-modified clay is used directly, the d-spacing is again similar at 3.2 – 3.5 nm. This strongly suggests that the structure of the clay counterion does not have a significant effect on nanocomposite formation. This is very different from what has been observed in bulk polymerization where the 10A clay gives an intercalated structure while VB16 is exfoliated [10].

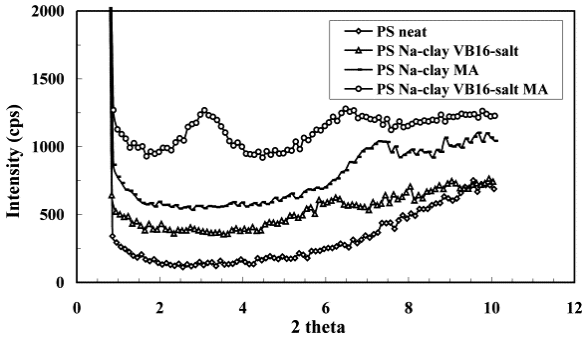

Fig. 4. XRD pattern of PS with VB16 salt and sodium clay and the effect of MA.

Attention is now turned to the effect of shear on nanocomposite formation. Fig. 5 shows the XRD results for the internal mixer while Fig. 6 shows those for the twin-screw extruder; the latter provides the most shear while the former is intermediate between the Brabender and the twin-screw. For the internal mixer, there is only a small difference between the direct use of the organically-modified clay versus the sodium clay plus the ammonium salt, as long as MA is present, the d-spacing is 3.1 nm for PS/VB16–clay/MA and 2.9 nm for PS/VB16-salt/Na-clay/MA. In the absence of MA, the d-spacing is significantly smaller, 2.1 nm for the organoclay and 1.9 nm for the sodium clay. In the twin-screw extruder, the devise with the highest shear rate, Fig. 6, the d-spacing increases by 0.4 nm for the VB16 clay in the presence of MA and by 0.1 nm in its absence; the presence of MA is apparently not important at higher shear rates.

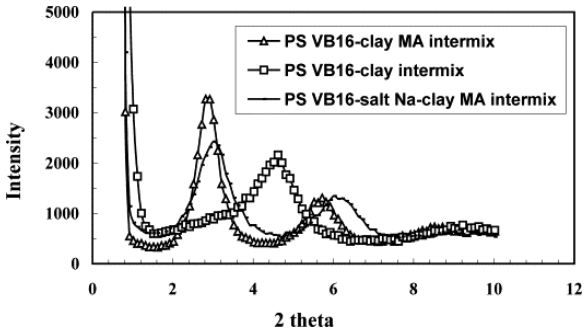

Fig. 5. XRD pattern of PS VB16–clay nanocomposite via intermixer.

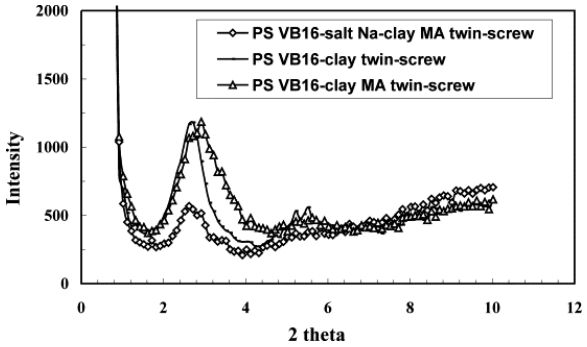

Fig. 6. XRD pattern of PS VB16 nanocomposite via twin-screw extruder.

The XRD results for PP systems prepared by the same procedures used for PS are now described. Fig. 7 shows the results for PP with the 10A clay and salt in the Brabender mixer. When the 10A clay is used a very small peak at 2ϑ=2.24, corresponding to a d-spacing of 3.9 nm, is observed. For the combination of PP with 10A salt and sodium clay, two small peaks are observed at 2ϑ=1.6 and 2.2, which correspond to a d-spacing of 5.5 nm and 4.0 nm. Since these are quite small peaks, this may indicate either a good deal of disorder or a mixed intercalated-exfoliated system. In the presence of MA, PP with sodium clay and 10A salt plus MA, a broad peak is observed at 2ϑ=6.5, the d-spacing is 1.4 nm; the d-spacing in the 10A clay is 1.9 nm. The sodium clay is apparently only partially converted to an organically-modified clay so nanocomposite formation does not occur.

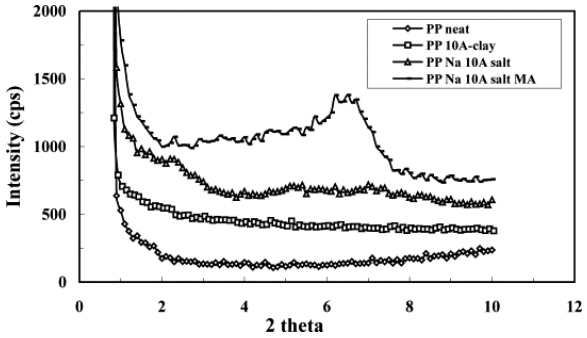

Fig. 7. XRD pattern of PP 10A–clay nanocomposite.

Fig. 8 gives the XRD pattern for VB16 systems. In all cases only broad peaks are seen, perhaps indicative of disorder in the system. For PP VB16 clay a broad peak from 2ϑ=2.2~5.0 is observed. The center appears to be at about 2ϑ=4.0, which gives a d-spacing somewhat smaller than in the pristine VB16 clay. For the PP–sodium clay–VB16 salt system, in the absence of MA no peak is seen, again probably indicative of disorder and not of an exfoliated system. When MA is added to this system, a fairly broad peak appears at 2ϑ=2.5, the d-spacing is 3.5 nm. This is a 2.3 nm increase compared to sodium clay and 0.6 nm increase compared to VB16 organic clay. This is clearly indicative of nanocomposite formation, probably with some disorder due to the breath of the peak.

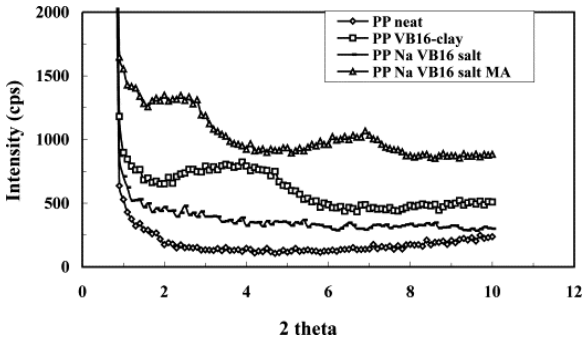

Fig. 8. XRD pattern of PP VB16–clay nanocomposite.

Fig. 9, Fig. 10 show the XRD results for PP melt blended in either the internal mixer or the twin-screw extruder. From the internal mixer, in the absence of MA only a small and very broad peak is observed, probably indicating disorder in the clay layers. When MA is present, the peak is at the same position and strong for both VB16 clay and sodium clay plus VB16 salt, 2.6 nm. In the case of the twin-screw, the peak position is a little lower than what is observed from the internal mixer. The largest d-spacing is observed for the blend of PP with the sodium clay, VB16 salt and MA (3.5 nm) but the value is 3.1 nm, not very different, for both the VB16 clay and that clay in the presence of MA. One may conclude that the greater shear of both the internal mixer and the twin-screw lead to larger peaks at greater d-spacing than is seen in the low shear Brabender mixer.

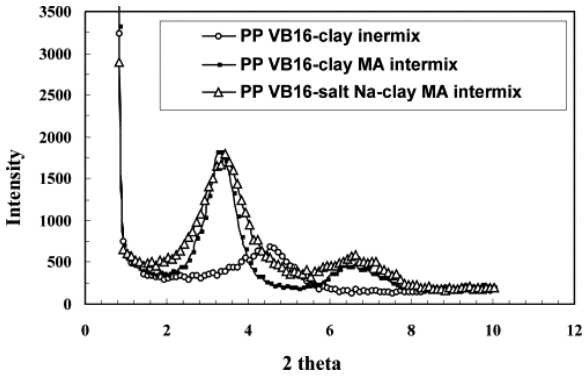

Fig. 9. XRD pattern of PP VB16–clay nanocomposite via intermixer.

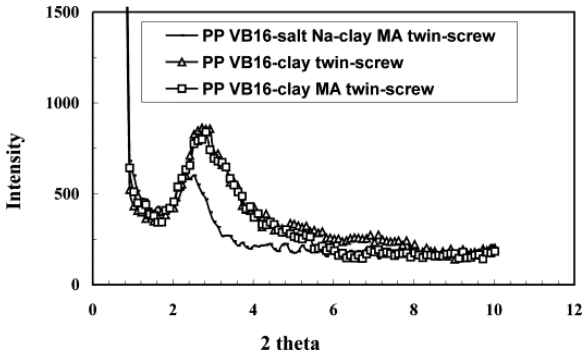

Fig. 10. XRD pattern of PP VB16–clay nanocomposite via twin-screw extruder.

3.2. Role of MA in in-situ reactive blending

The role of MA in the functionalization of PP has been previously considered [29], [30]. In the presence of a radical initiator, radical sites are formed on the PP chain and graft copolymerization of MA can occur at these sites. This leads to a functionalized polymer which may be better able to interact with the clay. Presumably a similar reaction must occur for PS.

3.3. Transmission electron microscopy (TEM)

XRD alone provides a description of the d-spacing in the clay but it does not show the actual image of the clay, this requires a technique such as TEM. Fig. 11, Fig. 12 show both the low and high magnification images of PS (Fig. 11) and PP (Fig. 12) nanocomposites. From the low magnification images one can see that there is not good dispersion of the clay throughout the polymer and that it is largely an immiscible material. The higher magnification images, on the other hand, clearly show discrete clay lines with polymer inserted between the clay layers. The d-spacing that may be calculated from these TEM images are in the range of 3.0–3.5 nm, in excellent agreement with XRD. These materials should probably be described as immiscible but there is polymer inserted between the clay layers.

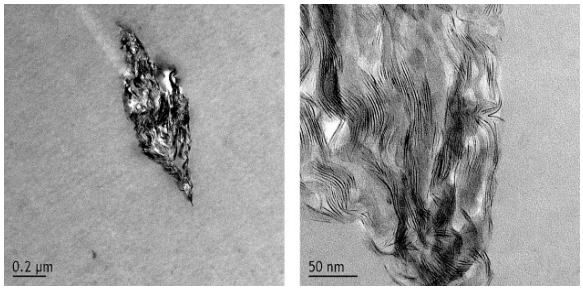

Fig. 11. Low (left) and high (right) magnification TEM images of PS/Na-clay nanocomposite (PS/Na-clay/VB-16 salt/MA) from the internal mixer.

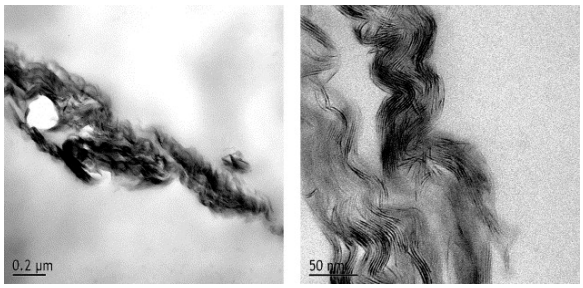

Fig. 12. Low (left) and high (right) magnification images of the PP/Na–clay nanocomposite (PP+MA+VB16 salt) from the internal mixer.

3.4. Thermogravimetric analysis (TGA)

The thermal stability of the nanocomposites has been accessed using TGA; the parameters for the PS nanocomposites (only those obtained from the Brabender mixer are included here) are shown in Table 1 and include the temperature at which 10% degradation occurs, a measure of the onset of degradation, the temperature at which 50% degradation occurs, the mid-point of the degradation process, and the fraction of material which remains at 600 °C, denoted as char [31]. The onset temperature of the degradation is about 10 – 30 °C higher for the nanocomposites than for pristine PS except for the PS–sodium clay–MA sample, where XRD indicates that there is essentially no change in the d-spacing and nanocomposite formation is unlikely to have occurred, and for PS–VB16 salt–sodium clay–MA, where XRD evidence would favor nanocomposite formation. Previous work with PS has shown that nanocomposite formation usually gives rise to a significant, ~50 °C, increase in onset temperature [10]. The changes in the temperature at which 50% degradation occur parallel the changes in onset temperature. The amount of non-volatile residue, char, is constant throughout the range and corresponds reasonably well to the amount of clay that has been added to the polymer.

Table 1. TGA results for reactive blending of PS–clay nanocomposites

Samples	10% (°C)	50% (°C)	Char (%)	XRD (nm)
PS	329	375	2	–
PS+Na-clay+MA	333	380	5	1.2
10A–clay	–	–	–	1.9
PS+10A–clay	349	398	6	3.5
PS+10A–clay+MA	360	404	6	3.2
PS+10A salt+Na-clay	343	392	4	1.5
PS+10A salt+Na-clay+MA	339	384	5	2.8
VB16–clay	–	–	–	2.9
PS+VB16–clay	351	392	5	2.1
PS+VB16–clay+MA	352	398	5	3.0
PS+VB16 salt+Na-clay	344	390	5	1.4

PS+VB16 salt+Na-clay+MA	328	377	5	2.9

For the PP system, in only two cases is the onset temperature enhanced relative to that in pristine PP, the PP–sodium clay–10A salt system and PP–10A clay. The presence of MA always causes a decrease in the onset temperature of the PP. In work from this laboratory we have found that the onset temperature in the TGA experiment for melt blended PP and PE is unaffected by nanocomposite formation [32] regardless of the clay used (Table 2). Once again the changes in the 50% temperature parallel those in the onset temperature and the amount of non-volatile residue correlates well with the amount of clay.

Table 2. TGA results for reactive blending of PP-clay nanocomposites

Sample	10% Mass loss	50% Mass loss	Char (%)
PP neat melt blended	337	413	4
PP Na 10A salt	367	432	5
PP Na 10A salt MA	322	411	6
PP 10A–clay	342	419	5
PP Na VB16 salt	337	418	5
PP Na VB16 salt MA	327	415	5
PP VB16–clay	331	417	5

3.5. Mechanical properties

An Instron test machine has been used to measure the tensile strength and elongation at break for both PS and PP nanocomposites; these results are shown in Table 3 for PS and Table 4 for PP. For PS samples that were mixed under the lowest shear condition, in the Brabender mixer, both the tensile strength and the elongation at break decrease, while when the samples were mixed under higher shear, both of these increase. Previous work has shown that there is not much change for PS nanocomposites, whether they are intercalated or exfoliated [14]. The enhanced properties seen in both the internal mixer and the twin-screw extruder certainly indicate that an interesting change has occurred.

Table 3. Tensile strength and elongation at break of PS–clay nanocomposites

Sample	Tensile strength (MPa)	Elongation at break (%)
PS neat	7.5[a]	12[a]
PS VB16–clay (Brabender)	4.9[a]	5[a]
PS 10A–clay (Brabender)	5.0[a]	5[a]
PS VB16–clay (Intermixer)	21.5[b]	54[b]
PS VB16–clay MA (Intermixer)	20.5[b]	56[b]
PS VB16 salt Na–clay MA (Intermixer)	26.1[b]	63[b]

aCrosshead speed 5 mm/min.
bCrosshead speed 1.25 mm/min.

Table 4. Tensile strength and elongation at break of PP–clay nanocomposites

Sample	Tensile strength (MPa)	Elongation at break (%)
PP neat melt blended (Brabender)	37.9[a]	1350[a]
PP 10A–clay (Brabender)	31.6[a]	143[a]
PP Na 10A salt MA (Brabender)	27.5[a]	1245[a]
PP VB16–clay (Brabender)	39.4[a]	36[a]
PP Na VB16 salt MA (Brabener)	32.4[a]	54[a]

PP VB16–clay (Intermixer)	25.0[b]	145[b]
PP VB16–clay MA (Intermixer)	23.6[b]	359[b]
PP VB16 salt Na-clay MA (Intermixer)	27.4[b]	526[b]

aCrosshead speed 5 mm/min.
bCrosshead speed 1.25 mm/min.

For polypropylene the tensile strength is always decreased and the elongation at break is very significantly reduced for all of these systems. Since these are apparently immiscible systems, the clay is acting primarily as a filler, and one may not expect to see enhanced mechanical properties.

3.6. Cone calorimetry

The assessment of the flammability of nanocomposites is usually by cone calorimetry; the parameters that are evaluated include the time to ignition, t_{ign}, the peak heat release rate, PHRR, and the time to PHRR, t_{PHRR}, the specific extinction area, SEA, a measure of smoke, and the mass loss rate, MLR. Observations that are usually made for nanocomposites are that the time to ignition is usually lower for nanocomposites than for the virgin polymer and that the PHRR is usually significantly decreased, with the amount of the decrease depending upon the particular polymer under investigation and not on the intercalated or exfoliated nature of the system. In general the amount of smoke is about the same or perhaps a little larger and the mass loss rate is decreased. The results for the polystyrene systems are presented in Table 5.

Table 5. Cone calorimeter results for PS reactive blending

Sample	t_{ign} (s)	PHRR (kW/m^2) (% reduction)	t_{PHRR} (s)	SEA (m^2/kg)	MLR (g/sm^2)
Brabender mixer					
PS	51	1450	92	875	37
PS-VB16–clay	38	997 (31)	98	947	32
PS-10A–clay	41	1102 (24)	93	855	33
PS-VB16–clay–MA	36	986 (32)	98	936	30
PS-10A–clay–MA	26	1003 (31)	87	900	30
PS-Na-clay–MA	29	1043 (28)	91	932	30
PS-Na-clay–MA–VB16 salt	32	1072 (26)	103	857	31
PS-Na-clay–MA–10A salt	31	1037 (28)	92	914	31
Internal mixer					
PS-VB16–clay	54	1127 (22)	88	1121	30
PS-VB16–clay–MA	44	1109 (24)	94	1121	28
PS-Na-clay–MA–VB16 salt	38	847 (42)	89	1183	22
Twin-screw extruder					
PS-VB16–clay	27	870 (40)	96	1199	23
PS-VB16–clay–MA	32	913 (37)	98	1228	25
PS-Na-clay–MA–VB16 salt	33	1050 (28)	96	1154	26

Looking first at the reduction in PHRR, the best that has been obtained is in the region of 50%. From the table we see that in most cases the reductions are in the 20–30% range and in only two or three cases do we even approach the 50% figure. This must be a reflection of the somewhat immiscible nature of this system. Gilman [27], [33] has reported that an immiscible PS-clay nanocomposite gives a 3% reduction while an intercalated system gives a 48% reduction. The values that are observed in this study are much closer to the high value and must indicate that nanocomposite formation has occurred. It should be noted that the time to PHRR is constant across the entire range of samples while the time to ignition does decrease and the greatest decrease in time to

ignition occurs for the systems which give the greatest reduction in PHRR. As expected the mass loss rate is decreased and the amount of smoke is constant to somewhat increased.

The cone calorimetric results for the polypropylene systems are shown in Table 6. There are no published results for simple polypropylene, rather results are available for polypropylene-graft-maleic anhydride. Notice must be directed to the entry for PP plus MA. The PHRR is routinely lower for this graft copolymer than for virgin PP. The value for virgin PP is 1600 kW/m^2, while PP-g-MA gives 1046 kW/m^2, both at an irradiance of 35 kW/m^2. Recently in this laboratory, we have been able to prepare an authentic, mixed intercalated-exfoliated nanocomposite of polypropylene. The reduction in PHRR for PP-g-MA [27], [33] is 54% while for PP itself [32], the best value that has been obtained is 20%. In this work the typical values are in the range of 11% up to 34%. If one compares with the unpublished value for PP, these results indicate that nanocomposite formation has occurred in those cases where the PHRR reduction is large. The mass loss rate does not change for all samples and the smoke is also relatively constant but there is a variation in time to ignition. The greatest decrease in time to ignition occurs for those systems which show the greatest reduction in PHRR. This may be a criteria for nanocomposite formation, a significant reduction in time to ignition and a significant reduction in PHRR. This suggests that a nanocomposite is formed with the 10A clay alone and with the sodium clay combined with the 10A salt, both with and without MA. There does not appear to be an advantage from the higher shear offered by the internal mixer or the twin-screw extruder.

Table 6. Cone calorimeter results for PP reactive blending

Sample	t_{ign} (s)	PHRR (kW/m^2)	t_{PHRR} (s)	SEA (m^2/kg)	MLR (g/s m^2)
Brabender mixer					
PP	49	1642	103	290	22
PP-VB16–clay	27	1246 (24)	102	283	22
PP-10A–clay	32	1084 (34)	108	281	21
PP–MA	27	1091 (34)	100	233	24
PS-Na–clay–MA–VB16 salt	30	1163 (29)	102	271	22
PS-Na–clay–MA–10A salt	26	1136 (31)	98	300	20
PP-Na–10A salt	23	1101 (33)	103	303	22
Internal mixer					
PP-VB16–clay	48	1420 (14)	108	386	22
PP-VB16–clay–MA	46	1456 (11)	106	354	23
PP-Na–clay–MA–VB16 salt	46	1278 (22)	114	380	20
Twin-screw extruder					
PP-VB16–clay	32	1344 (18)	108	316	21
PP-VB16–clay–MA	34	1197 (27)	100	327	20
PS-Na–clay–MA–VB16 salt	34	1351 (18)	105	327	20

4. Conclusions

PS– and PP–clay nanocomposites have been prepared by in situ reactive blending both with organic clay and sodium clay in the presence of maleic anhydride (MA). From XRD the d-spacing increases to a value larger than 3 nm. TEM shows that the clay is non-homogenously distributed throughout the polymer but polymer is inserted between the clay layers and the d-spacing agrees with that found by XRD. Thermal degradation in nitrogen in a little more difficult for the PS systems and is not effected for PP materials. The cone calorimetric results show that there is a significant reduction in peak heat release rate, much larger than would be expected from an immiscible system but not quite as large as has been observed for true intercalated or exfoliated PS nanocomposites. This suggests that the systems are at least partially intercalated, in agreement with the

observations from XRD and TEM, and that the fact that the clay is not homogeneously distributed does not mean that one cannot describe this as a nanocomposite. The presence of maleic anhydride during the melt blending seems to enhance intercalation.

Acknowledgements

This work was performed under the sponsorship of the US Department of Commence, National Institute of Standards and Technology, Grant Number 70NANB6D0119. The assistance of Alexander Morgan and Joseph Harris at the Dow Chemical Company in obtaining the TEM images is gratefully acknowledged. The cooperation of Tie Lan and Jerry Qian at Nanocor, Inc., in making their internal mixer and twin screw extruder available is greatly appreciated.

References

[1] E.P. Giannelis, R. Krishnamoorti, E. Manias. *Adv Polym Sci*, 138 (1999), pp. 107-147
[2] A. Alexandre, P. Dubois. *Mater Sci Eng*, 28 (2000), pp. 1-63
[3] T.J. Pinnavaia, G.W. Beall ***Polymer–clay nanocomposites.*** Wiley, New York (2001)
[4] C.O. Oriakhi, M.M. Lerner. *Mater. Res. Bull*, 30 (1995), p. 723
[5] H. Nakajima, G.M. Ubayashi. *J. Mater. Chem*., 5 (1995), p. 105
[6] T. Lan, T.J. Pinnavaia. *Chem. Mater*., 6 (1994), p. 573
[7] D. Wang, D. Parlow, Q. Yao, C.A. Wilkie. *J. Vinyl Add. Tech*.nol, 7 (2001), pp. 203-213
[8] Wang, D, Parlow D, Yao Q, Wilkie CA. *J. Vinyl Add Technol* 2002;8:139–50.
[9] N. Ogata, S. Kawakage, T. Ogihara. *J. Appl. Polym. Sci*., 66 (1997), pp. 573-581
[10] J. Zhu, A.B. Morgan, F.J. Lamelas, C.A. Wilkie. *Chem Mater*., 13 (2001), pp. 3774-3780
[11] C.-R. Tseng, J.-Y. Wu, H.-Y. Lee, F.-C. Chang. *Polymer*, 42 (2001), pp. 10063-10070
[12] X. Fu, S. Qutubuddin. *Mater. Lett*., 42 (2000), pp. 12-15
[13]. M.W. Noh, D.C. Lee. *Polym. Bull. (Berlin),* 42 (1999), pp. 619-626
[14] Wang D, Zhu J, Yao Q, Wilkie CA. *Chem Mater* 2002;14:3837–43.
[15] C. Zeng, L.J. Lee. *Ann. Tech. Conf. Soc. Plast. Eng.* (2) (2001), pp. 2213-2220
[16] C. Zeng, L.J. Lee. *Macromolecules*, 34 (2001), pp. 4098-4103
[17] G.-M. Chen, Y.-M. Ma, Z.-N. Qi. Gaodeng Xuexiao Huaxue Xuebao [*Journal of Chinese University Chemistry*], 22 (2001), pp. 872-874
[18] C.I. Park, O.O. Park, J.G. Lim, H.J. Kim. *Polymer*, 42 (2001), pp. 7465-7475
[19] X. Liu, Q. Wu. *Polymer*, 42 (2001), pp. 10013-10019
[20] P.H. Nam, P. Maiti, M. Okamoto, T. Kotaka, N. Hasegawa, A. Usuki. *Polymer*, 42 (2001), pp. 9633-9640
[21]M. Okamoto, P.H. Nam, P. Maiti, T. Kotaka, T. Nakayama, M. Takada, M. Oshima, A.Usuki, N. Hasegawa, H. O kamoto. *Nano Lett*., 1 (2001), pp. 503-505
[22] P. Kodgire, R. Kalgaonkar, S. Hambir, N. Bulakh, J.P. Jog. *J. Appl. Polym. Sci.,* 81 (2001), pp. 1786-1792
[23] S. Hambir, N. Bulakh, P. Kodgire, R. Kalgaonkar, J.P. Jog. *J. Polym. Sci., Part B: Polym. Phys,* 39 (2001), pp. 446-450
[24] J. Kim, J.S. Lee, J.W. Lee. *Proc. Int. Congr. Rheol*. 13th, 4 (2000), pp. 33-35
[25] S. Lee, J.S. Park, H. Lee. *Polym. Mater. Sci. Eng*., 83 (2000), p. 417
[26] Y. Kurokawa, H. Yasuda, A. Oya. *J. Mater. Sci. Lett*., 15 (1996), pp. 1481-1483
[27] Gilman JW, Kashiwagi T, Nyden M, Brown JET, Jackson CL, Lomakin S, et al. In: Al-Maliaka S, Golovoy A, Wilkie CA, editors. *Chemistry and technology of polymer additives*. London: Blackwell Scientific; 1998. p. 249–65.
[28] M. Alexandre, G. Beyer, C. Henrist, R. Cloots, A. Rulmont, R. Jerome, P. Dubois. *Chem Mater*., 13 (2001), pp. 3830-3832

[29] S.-H. Lee, K. Yang. *Polym Sci Technol*., 9 (1998), pp. 193-199
[30] Du Shi-guo, Shi Dong-mei, Deng Hui, Hua Xue Shi Jie [*Chemistry World*], 2000, 413, 115–20 [in Chinese].
[31] J. Zhu, P. Start, K.A. Mauritz, C.A. Wilkie. *J. Polym. Sci., Part A: Polym. Chem*., 40 (2002), pp. 1498-1503
[32] Su S, Wilkie CA. Unpublished observations.
[33] Gilman JW, Kashiwagi T, Giannelis EP, Manias E, Lomakin S, Lichtenhan JD, Jones P. In: LeBras M, Camino G, Bourbigot S, Delobel R, editors. Fire retardancy of polymer, the use of intumescence. *Royal Society of Chemistry*; 1998. p. 203–21.